Letter

Multiple dimensions of spin-gapless semiconducting states in tetragonal Sr_2CuF_6

Jianhua Wang,[1,*] Hongkuan Yuan,[1,*] Ying Liu,[2,†] Xiaotian Wang,[1,‡] and Gang Zhang[3,§]
[1]*School of Physical Science and Technology, Southwest University, Chongqing 400715, China*
[2]*School of Materials Science and Engineering, Hebei University of Technology, Tianjin 300130, China*
[3]*Institute of High Performance Computing, Agency for Science, Technology and Research (A*STAR), Singapore 138632, Singapore*

(Received 21 June 2022; revised 7 August 2022; accepted 11 August 2022; published 22 August 2022)

Spin-gapless semiconductors (SGSs), with intrinsic magnetism, 100% spin polarization, and zero-gap band crossing points, have attracted great scientific interest owing to their potential applications in spintronics. In this Letter, using first-principles calculations and symmetry analysis, we demonstrate that the realistic material Sr_2CuF_6 is a spintronic material with multiple dimensions of spin-gapless semiconducting states. Tetragonal Sr_2CuF_6 has a zero-dimensional zero-gap nodal point, a one-dimensional zero-gap nodal line, and a two-dimensional nearly zero-gap nodal surface in one spin direction. Moreover, it hosts a wide band gap in the other spin direction. Our results extend the SGS members from nodal point SGSs and nodal line SGSs to nodal surface SGSs. Furthermore, we report a SGS candidate in an experimentally realized material exhibiting different dimensions of zero-gap points in momentum space. It is hoped that spintronic materials with multiple dimensions of spin-gapless semiconducting states may have significant applications in new-generation spintronics.

DOI: 10.1103/PhysRevB.106.L060407

Introduction. Spintronics [1,2] is one of the most promising next-generation information technologies. It uses the electron spins as information carriers and has the potential advantages of accelerating data processing, high circuit integration density, and low-energy consumption. Owing to these advantages, new classes of spintronic materials have been proposed one after another [3–8]. In 2008, Wang [9] proposed a new type of zero-gap material, that is, a spin-gapless semiconductor (SGS) with 100% spin-polarized carriers, high carrier mobility, and zero (or negligible) low excitation energy of electrons from the valence band to the conduction band. Motivated by this work, several SGSs [10–15] with a zero-gap state and parabolic or linear energy-momentum dispersions were predicted using first-principles calculations. Moreover, the SGS behaviors in some well-known Heusler alloys, such as Mn_2CoAl [16], CoFeCrGe [17], and CoFeMnSi [18] with parabolic energy-momentum dispersions, have been confirmed by measuring the transport properties through experiments. The origin of the SGS behavior in Heusler alloys based on the Slater-Pauling rule and a semiempirical general rule for designing Heusler-based SGSs, in theory, are discussed in Ref. [12]. Xu *et al.* [19] proposed a new spin injection scheme based on SGSs and typical semiconductors that can retain the high-spin polarization of the injection source and overcome the conducting mismatch between the half metals and typical semiconductors.

In addition to designing the Heusler-based SGSs with parabolic energy-momentum dispersions mentioned above, researchers have also made significant efforts in designing SGSs with linear energy-momentum dispersions. Among them, SGSs with a zero-dimensional (0D) nodal point [20–24] and a one-dimensional (1D) nodal line [25–29] in momentum space are of great importance and have very recently attracted significant attention. Dirac-point SGSs [30,31] are mainly proposed among two-dimensional (2D) materials, and they possess fundamental massless Dirac fermions and dissipationless transport properties. The 2D Dirac SGSs have yet to be experimentally realized because they are monolayer materials; hence, they are hard to synthesize. Moreover, some monolayer materials are not stable in the ambient environment. Thus, new nanotechnology is needed for fabricating monolayer Dirac-point SGSs. Dirac-point SGSs have isolated 0D band crossing points at the Fermi level and in momentum space. In 2020, Zhang *et al.* [25] proposed nodal line SGSs [32] in three-dimensional (3D) solids. For nodal line SGSs, the band crossing points at the Fermi level are not isolated and can form a 1D line or a geometry, which is formed by more than one 1D line, in momentum space. Nodal line SGSs possess 100% spin polarization, high carrier mobility, zero-gap nodal line states at the Fermi level in one spin direction, and spin-polarized hallmark drumhead surface states. In a review of recent advances in the field of nodal line SGSs, Ding *et al.* [26] reported that a series of 2D and 3D materials, which are potential nodal line SGSs, has been proposed in the last five years. They have also suggested some theoretical prediction approaches for 3D nodal line SGSs as future prospects, which is encouraging.

The outcomes of the studies mentioned above lead to some interesting questions: (1) Is it possible to find a nodal surface SGS with zero-gap band crossing points at the Fermi level that can form a 2D nodal surface in momentum space? (2) If yes, then is it possible to find a realistic material that can

*These authors contributed equally to this work.
†Corresponding author: ying_liu@hebut.edu.cn
‡Corresponding author: xiaotianwang@swu.edu.cn
§Corresponding author: zhangg@ihpc.a-star.edu.sg

cohost 0D nodal point, 1D nodal line, and 2D nodal surface spin-gapless semiconducting states? In this Letter, we address the above questions. We select tetragonal Sr_2CuF_6 with a $P\bar{4}b2$ structure and space group (SG) 117 as an example to discuss the 0D nodal point, 1D nodal line, and 2D nearly nodal surface spin-gapless semiconducting states in its band structure. Sr_2CuF_6 is a prepared material [33] whose crystal structure was determined in 1970. Moreover, we show that the multiple dimensions of spin-gapless semiconducting states in tetragonal Sr_2CuF_6 are robust to uniform strains and the on-site Hubbard Coulomb interaction. This Letter proposes, in theory, a nearly nodal surface SGS and reveals a realistic material with multiple dimensions of spin-gapless semiconducting behaviors. Moreover, this study discusses possible alternative physics and potential applications of SGSs with different dimensions of zero-gap band crossing points in momentum space.

Ground state and electronic structure. Before calculating the electronic structure of tetragonal Sr_2CuF_6, we determined the magnetic ground state for Sr_2CuF_6. Figure S1 [see Supplemental Material (SM) [34]] shows the energy comparison of Sr_2CuF_6 under four collinear magnetic configurations, including one ferromagnetic, two antiferromagnetic, and one nonmagnetic configurations. The arrows in Fig. S1 indicate the spin directions of the Cu atoms. It can be seen in Fig. S1 that the ferromagnetic configuration is the ground state for Sr_2CuF_6, because the ferromagnetic configuration has lower energy than the other three magnetic configurations. The total magnetic moment (M_t) of Sr_2CuF_6 is $4\,\mu_B$, and the main contribution to the total M_t is from the Cu atoms (see Table S1 in SM [34]). The magnetic moments listed in Table S1 are computed by placing a sphere around each atom with the radius given in Table S2 (see SM [34]). The optimized lattice constants for ferromagnetic Sr_2CuF_6 are $a = b = 5.807$ Å and $c = 16.558$ Å, which correspond well with the experimental data ($a = b = 5.710$ Å and $c = 16.458$ Å) [33]. The Sr, Cu, and F atoms are located at the $4f/4e$, $2a/2d$, and $8i$ Wyckoff sites, respectively [see Fig. 1(a) and Table S3 in SM [34]].

Based on the selected high-symmetry paths Γ-X-M-Γ-Z-R-A-$Z|X$-$R|M$-A [Fig. 1(b)], the spin-polarized band structures for ferromagnetic Sr_2CuF_6 at the equilibrium lattice constants are shown in Figs. 1(c) and 1(d). It can be seen that the bands in the spin-up direction exhibit a semiconducting behavior. A large energy gap of 4.34 eV appears in the spin-up direction. Moreover, the bands in the spin-down direction exhibit a metallic behavior and overlap with the Fermi level, forming various band crossing points with ultraclean energy dispersions that are, without other rambling bands nearby, along Γ-X, M-Γ, Z-R, and A-Z, at the Fermi level. Interestingly, as shown in Fig. 1(d), these band crossing points along Γ-X, M-Γ, Z-R, and A-Z are zero-gap band crossing points, that is, the lowest conduction band and the highest valence band cross at the Fermi level along Γ-X, M-Γ, Z-R, and A-Z [in regions A and C of Fig. 1(d)]. Hence, ferromagnetic Sr_2CuF_6 is a typical SGS with linear energy-momentum dispersions at the Fermi level [Fig. 2(a)] [9,62]. As a SGS, Sr_2CuF_6 shows 100% spin polarization [64] and it may have applications as a spin-polarized current source for magnetic tunneling junctions and spin injectors

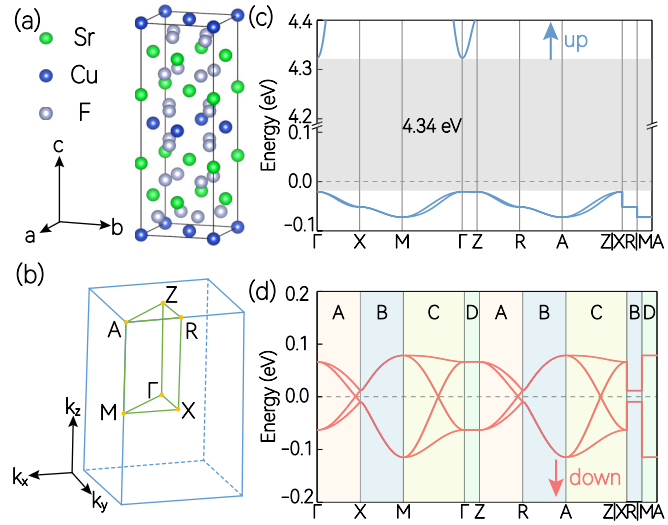

FIG. 1. (a) Crystal structure of Sr_2CuF_6. (b) Three-dimensional Brillouin zone and some high-symmetry points. (c) and (d) Spin-up and spin-down band structures for Sr_2CuF_6, respectively. The dotted lines in (c) and (d) represent the positions of the Fermi level.

to semiconductors. In the spin-down direction of Sr_2CuF_6, besides the multiple zero-gap band crossing points at the Fermi level, the magnetic Weyl (in region B) and quadratic (in region D) nodal lines [63,65] coexist around the Fermi level (see Figs. S2–S4, and the discussion in SM [34]). Furthermore, the effects of an on-site Hubbard Coulomb

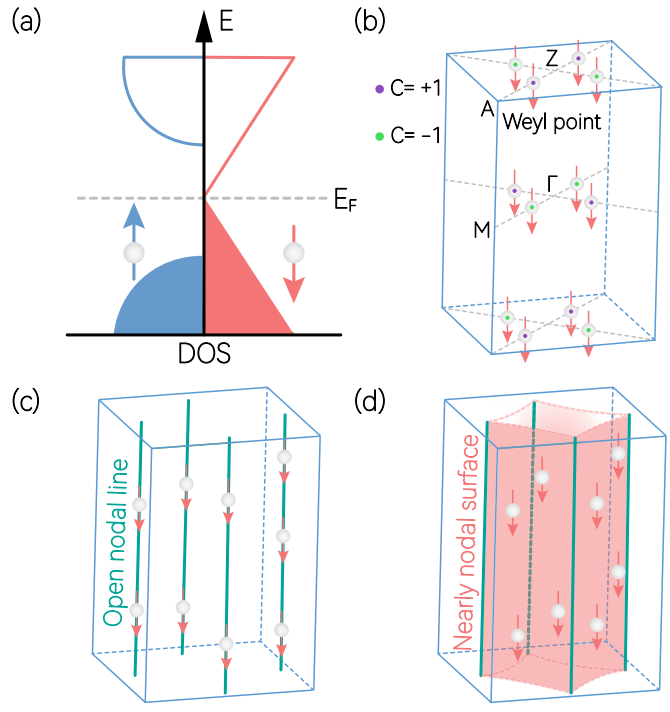

FIG. 2. (a) Schematic illustration of the spin-polarized band structure of SGS with linear-type zero-gap band crossing points. (b)–(d) Schematic illustration of the 0D Weyl point, 1D open nodal line, and 2D nearly nodal surface spin-gapless semiconducting states in the 3D Brillouin zone of Sr_2CuF_6.

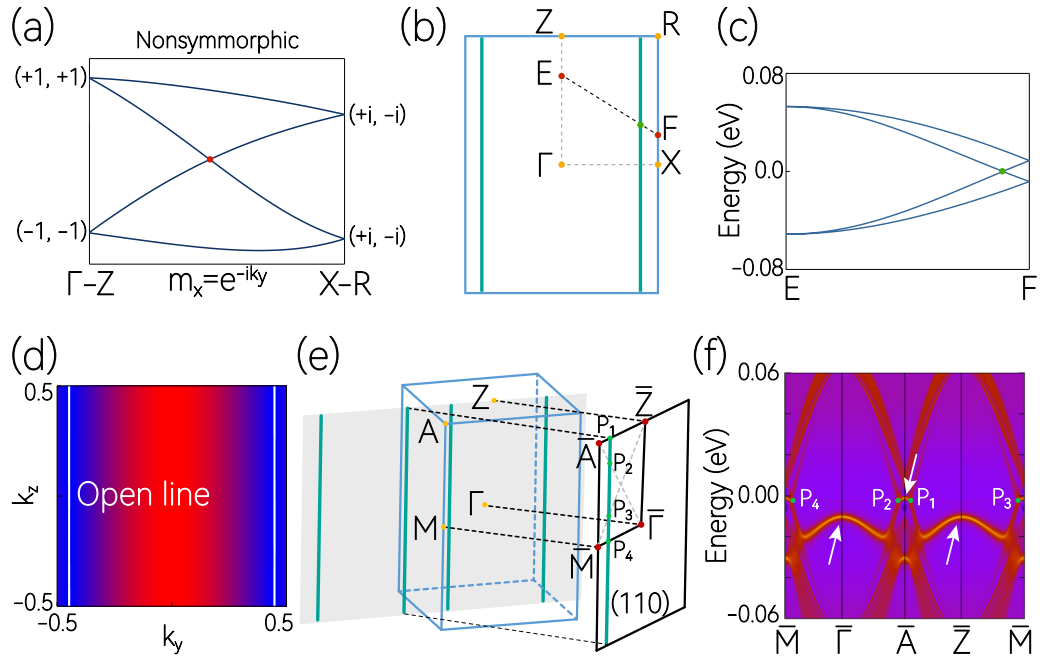

FIG. 3. (a) Schematic illustration of hourglass dispersions along the nonsymmorphic path. (b) Selected E-F path and (c) the spin-down band structure for Sr_2CuF_6 along the E-F path. (d) Shapes of the open lines in the $k_x = 0$ plane calculated by DFT. (e) 3D Brillouin zone and the projected (110) surface. The open nodal line of the extended Brillouin zone is projected onto the (110) plane. (f) Surface spectrum for the (110) surface along the $\overline{M}$-$\overline{\Gamma}$-$\overline{A}$-$\overline{Z}$-$\overline{M}$ surface paths. The projections of P1–P4, corresponding to the open nodal line in the bulk, are represented by green circles.

interaction, uniform strain, and the spin-orbit coupling (SOC) for the multiple zero-gap band crossing points at the Fermi level are shown in Figs. S5 and S6 in SM [34].

The lattice structure of Sr_2CuF_6 belongs to SG 117 that is generated by a twofold rotation symmetry C_{2z}, glide mirror $\widetilde{M}_y : (x + \frac{1}{2}, -y + \frac{1}{2}, z)$, and S_{4z} rotation symmetry. In addition, the lattice structure also has a glide mirror $\widetilde{M}_x : (-x + \frac{1}{2}, y + \frac{1}{2}, z)$ when considering a combination of generating elements. Because this system has a ferromagnetic ground state, the spin-up and spin-down states are separated. Notably, the states around the Fermi level are fully spin polarized; thus, we focused on the zero-gap points at the Fermi level in the spin-down direction and showed the 0D nodal point, 1D nodal line, and 2D nearly nodal surface spin-gapless semiconducting states in the spin-down band structure of Sr_2CuF_6.

0D spin-gapless semiconducting states. In region C of Fig. 1(d), two obvious zero-gap band crossing points along the M-Γ and A-Z high-symmetry paths can be observed. Around the Fermi level, four bands are present, and the band connections of the two band crossing points exhibit a typical hourglass shape [66–70]. The two band crossing points at the Fermi level are isolated magnetic Weyl points with the absolute value of Chern number equal to 1, i.e., $|C| = 1$. Figure 2(b) shows the schematic diagram of multiple 0D Weyl point spin-gapless semiconducting states in Sr_2CuF_6. The blue and green dots represent the locations of the multiple spin-down Weyl points with $C = +1$ and $C = -1$, respectively, in the 3D Brillouin zone.

It is noteworthy that the Weyl points on the high-symmetry lines M-Γ and A-Z are accidental degeneracies associated with rotation symmetries such as C_{2a}. To confirm this, our calculations indicated that the irreducible representations for the crossing bands are $\{\Sigma_1, \Sigma_2\}$, which are characterized by opposite eigenvalues of C_{2a}. Consequently, their crossings are stabilized by C_{2a}.

1D spin-gapless semiconducting states. In region A of Fig. 1(d), two obvious zero-gap band crossing points along the Γ-X and Z-R paths are observed. Owing to the presence of $\widetilde{M}_x$, these two band crossing points are not isolated but belong to a nodal line in the $k_x = 0$ plane, as shown in Fig. 3(b). In Fig. 3(b), we selected the E-F symmetry path, and E and F are points on the Z-Γ and R-X paths, respectively. The spin-down band structure along the E-F path is shown in Fig. 3(c). Similar to the band structures along the Z-R and Γ-X paths, an hourglass-shaped zero-gap band crossing point appears at the Fermi level. Using the first-principles calculation, we screen the shape of the line in the $k_x = 0$ plane, and the results are shown in Fig. 3(d). The open nodal lines, which traverse in the k_z direction of the bulk Brillouin zone and are formed by the zero-gap band crossing points with an hourglass dispersion, are apparent. Figure 2(c) shows the schematic diagram of 1D open nodal line spin-gapless semiconducting states in Sr_2CuF_6, in which the green lines represent the spin-down open nodal lines in the 3D Brillouin zone.

The open nodal lines on the $k_x = 0$ plane are formed by band switching between two bands enforced by a glide mirror. The plane $k_x = 0$ is the invariant subspace of $\widetilde{M}_x$; thus, each Bloch state $|u\rangle$ on the plane can be chosen as the eigenvalues of $\widetilde{M}_x$. In addition, on the plane $k_x = 0$, $\widetilde{M}_x^2 = e^{-ik_y}$. Hence, the eigenvalues of $\widetilde{M}_x$ are given by $g_x = \pm e^{-\frac{ik_y}{2}}$, which is k dependent. It is noteworthy that although the time-reversal symmetry ($\mathcal{T}$) is broken for the ferromagnetic system, we still

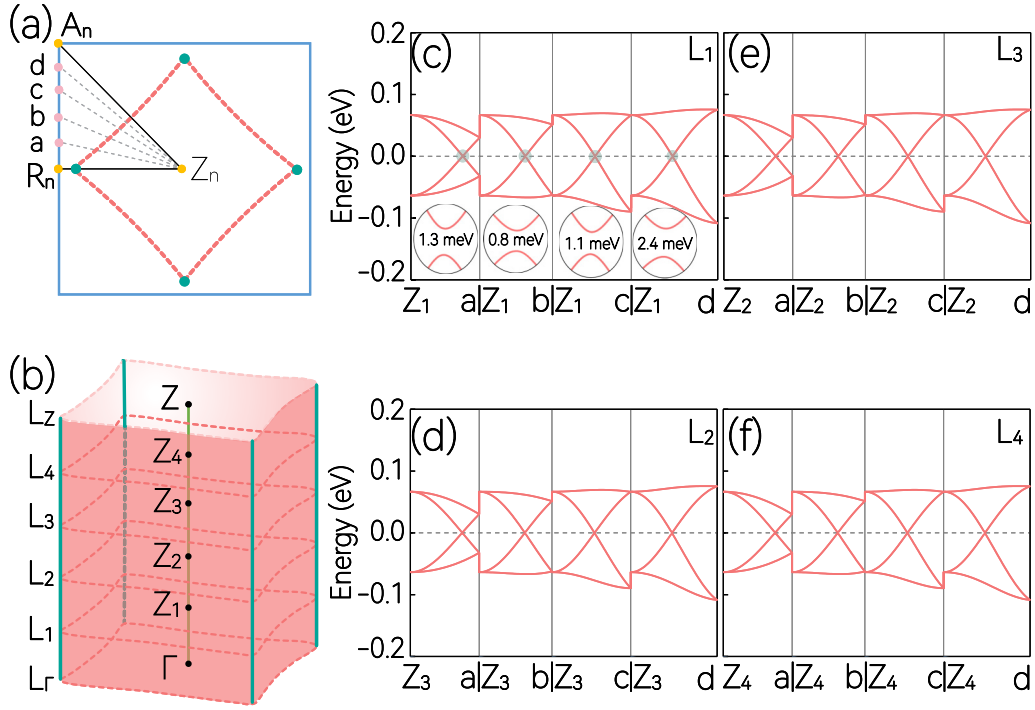

FIG. 4. (a) Selected Z_n-$a/b/c/d$ paths of the L1–L4 planes. The green dots represent the zero-gap band crossing points from the open nodal lines, while the red dotted lines show the nearly nodal line formed by the nearly zero-gap band touching points. (b) Schematic illustration of an open square cylinder nearly nodal surface (highlighted by the red color) and the open nodal lines (green lines) in the 3D Brillouin zone. (c)–(f) Spin-down band structures along the Z_n-$a/b/c/d$ ($n = 1, 2, 3, 4$) paths of the L1–L4 planes.

consider its presence only when focusing on one spin channel, that is, $\mathcal{T} = \mathcal{K}$, where $\mathcal{K}$ is the complex conjugation. In addition, the path Γ-Z is invariant under a combined operation $(S_{4z}\mathcal{T})^2 = -1$, manifesting a Kramers-like degeneracy. On this path, two 1D irreducible representations exist that could be related by $S_{4z}\mathcal{T}$ degeneracy, leading to a nodal line. In addition, $S_{4z}\widetilde{M}_x = \widetilde{M}_x S_{4z}^3$, such that the Kramers-like partners $|u\rangle$ and $S_{4z}\mathcal{T}|u\rangle$ have the same eigenvalues. A 2D irreducible representation exists on the path X-R, with the eigenvalues of $\widetilde{M}_x$ equal to $\pm i$. Consequently, owing to different pairings from Γ-Z to X-R, there must be a partner switching from path Γ-Z to X-R, forming an hourglass band dispersion [Fig. 3(a)]. Owing to the presence of the mirror symmetry, such an hourglass point is not isolated but belongs to a point on a nodal line, as shown in Figs. 3(b) and 3(d).

In Fig. 3(e), we projected one open nodal line, which belongs to the extended Brillouin zone, into the (110) plane. As shown in Fig. 3(f), P1–P4 are the projections of some zero-gap band crossing points of the open nodal line. The surface spectrum of the (110) surface along the $\overline{M}$-$\overline{\Gamma}$-$\overline{A}$-$\overline{Z}$-$\overline{M}$ path is shown in Fig. 3(f). Indeed, the surface states (the lines marked with white arrows) can be depicted from the projections of the zero-gap band crossing points (P1–P4).

2D nearly spin-gapless semiconducting states. In Fig. 4(b), we selected L1–L4 planes, which are normal to the k_z axis. In each plane, some symmetry paths, Z_n-$a/b/c/d$ ($n =$ 1-4), were selected [see Fig. 4(a)]. The spin-down band structures along the Z_n-$a/b/c/d$ paths of L1–L4 planes are shown in Figs. 4(c)–4(f). From Figs. 4(c)–4(f), it is evident that a series of zero-gap points exist along the Z_n-$a/b/c/d$ ($n =$ 1-4) paths. However, these zero-gap points are not under the protection of symmetry and they exist because the lowest conduction band and the highest valence band of the same spin component have their extreme values at the same k points and at the Fermi level. Hence, in this study, we used band touching points instead of band crossing points to describe the zero-gap points along the Z_n-$a/b/c/d$ paths of the L1–L4 planes. Due to the Pauli repulsion, the lowest conduction band and the highest valence band of these band touching points cannot absolutely touch at the Fermi level [27], that is, the almost negligible value of the opened gaps can be observed. As shown in Fig. 4(c), the value of the opened gaps for these band touching points is up to 2.4 meV, which is below the resolution of angle-resolved photoemission spectroscopy and significantly less than the energy scale of room temperature (26 meV).

Figure 4(a) shows a schematic illustration of a nearly nodal loop on one of the Z_n paths. The green dots represent the zero-gap band crossing points (from the open nodal lines and under the protection of symmetry), whereas the red dotted lines represent the nearly nodal lines (formed by the nearly zero-gap band touching points and not protected from the symmetry). Nearly nodal loops formed by the zero-gap band crossing points and nearly zero-gap band touching points with an hourglass-shaped dispersion in every plane normal to the k_z axis can be observed, resulting in a 2D nearly nodal surface [71–80] in momentum space [Fig. 4(b)]. Thus, ferromagnetic Sr_2CuF_6 is a SGS with 2D nearly spin-gapless semiconducting states [Fig. 2(d)]. The following points are noteworthy: (i) The nearly nodal surface structure is an open square cylinder traversing in the k_z direction of the bulk Brillouin zone direction. (ii) In experiments, the nearly nodal surface structure

in Sr_2CuF_6 is intrinsic and does not require any external conditions, such as electric field, pressure, doping, or element substitution. (iii) The band touching points forming the nodal surface are nearly flat in energy and fully spin polarized. It is well known that the coarse-grained quasiparticles, excited from a nodal surface, have intrinsic pseudospin degrees of freedom [71] and unique plasmonic behaviors [81]. Moreover, the nodal surface SGSs provide a magnetic platform to realize the spin-polarized nodal surface states and investigate their spintronic properties.

Conclusion. In this Letter, we extended the SGS family from SGSs with 0D nodal points and SGSs with 1D nodal lines to SGSs with 2D nearly nodal surfaces. Furthermore, we considered an example of a realistic material, Sr_2CuF_6, to demonstrate the coexistence of 0D nodal point, 1D nodal line, and 2D nodal surface spin-gapless semiconducting states within the material. Sr_2CuF_6 exhibits several exotic physical behaviors, including different spin-polarized zero-gap nodal structures in momentum space, 100% spin polarization, and a spin-polarized surface spectrum (arising from the zero-gap band crossing points of the open nodal line). This work can help enrich the diversity of spintronic materials and promote the development of next-generation spintronics.

Acknowledgments. X.W. is grateful for the support from the National Natural Science Foundation of China (No. 51801163). Y.L. is grateful for the support from 100 Talents Plan of Hebei Province (No. E2020050014) and the Nature Science Foundation of Hebei Province (No. A2021202002). H.Y. is grateful for the support from the the National Natural Science Foundation of China (11874306, 12174320) and the Natural Science Foundation of Chongqing (cstc2021jcyj-msxmX0209, cstc2022ycjh- bgzxm0127).

[1] S. A. Wolf, D. D. Awschalom, R. A. Buhrman, J. M. Daughton, S. Von Molnar, M. L. Roukes, A. Y. Chtchelkanova, and D. M. Treger, Science **294**, 1488 (2001).
[2] I. Žutić, J. Fabian, and S. D. Sarma, Rev. Mod. Phys. **76**, 323 (2004).
[3] M. I. Katsnelson, V. Yu. Irkhin, L. Chioncel, A. I. Lichtenstein, and R. A. de Groot, Rev. Mod. Phys. **80**, 315 (2008).
[4] X. Li, X. Wu, Z. Li, J. Yang, and J. Hou, Nanoscale **4**, 5680 (2012).
[5] K. Sato, L. Bergqvist, J. Kudrnovsky, P. H. Dederichs, O. Eriksson, I. Turek, B. Sanyal, G. Bouzerar, H. Katayama-Yoshida, V. A. Dinh, T. Fukushima, H. Kizaki, and R. Zeller, Rev. Mod. Phys. **82**, 1633 (2010).
[6] D. F. Liu, A. J. Liang, E. K. Liu, Q. N. Xu, Y. W. Li, C. Chen, D. Pei, W. J. Shi, S. K. Mo, P. Dudin, T. Kim, C. Cacho, G. Li, Y. Sun, L. X. Yang, Z. K. Liu, S. S. P. Parkin, C. Felser, and Y. L. Chen, Science **365**, 1282 (2019).
[7] N. Morali, R. Batabyal, P. K. Nag, E. Liu, Q. Xu, Y. Sun, B. Yan, C. Felser, N. Avraham, and H. Beidenkopf, Science **365**, 1286 (2019).
[8] Z. Yue, Z. Li, L. Sang, and X. Wang, Small **16**, 1905155 (2020).
[9] X. L. Wang, Phys. Rev. Lett. **100**, 156404 (2008).
[10] Y. F. Li, Z. Zhou, P. W. Shen, and Z. F. Chen, ACS Nano **3**, 1952 (2009).
[11] X. Li and J. Yang, Natl. Sci. Rev. **3**, 365 (2016).
[12] X. Wang, Z. Cheng, J. Wang, X.-L. Wang, and G. Liu, J. Mater. Chem. C **4**, 7176 (2016).
[13] Q. Gao, I. Opahle, and H. Zhang, Phys. Rev. Materials **3**, 024410 (2019).
[14] E. Şaşıoğlu, T. Aull, D. Kutschabsky, S. Blügel, and I. Mertig, Phys. Rev. Applied **14**, 014082 (2020).
[15] A. Jakobsson, P. Mavropoulos, E. Şaşıoğlu, S. Blügel, M. Ležaić, B. Sanyal, and I. Galanakis, Phys. Rev. B **91**, 174439 (2015).
[16] S. Ouardi, G. H. Fecher, C. Felser, and J. Kübler, Phys. Rev. Lett. **110**, 100401 (2013).
[17] L. Bainsla, A. I. Mallick, M. M. Raja, A. A. Coelho, A. K. Nigam, D. D. Johnson, A. Alam, and K. G. Suresh, Phys. Rev. B **92**, 045201 (2015).
[18] L. Bainsla, A. I. Mallick, M. M. Raja, A. K. Nigam, B. S. D. C. S. Varaprasad, Y. K. Takahashi, A. Alam, K. G. Suresh, and K. Hono, Phys. Rev. B **91**, 104408 (2015).
[19] G. Z. Xu, X. M. Zhang, Z. P. Hou, Y. Wang, E. K. Liu, X. K. Xi, S. G. Wang, W. Q. Wang, H. Z. Luo, W. H. Wang, and G. H. Wu, Europhys. Lett. **111**, 68003 (2015).
[20] X. Wang, T. Li, Z. Cheng, X.-L. Wang, and H. Chen, Appl. Phys. Rev. **5**, 041103 (2018).
[21] X.-L. Wang, Natl. Sci. Rev. **4**, 252 (2017).
[22] Q. L. Sun, Y. D. Ma, and N. Kioussis, Mater. Horiz. **7**, 2071 (2020).
[23] A. Wang, X. Zhang, Y. Feng, and M. Zhao, J. Phys. Chem. Lett. **8**, 3770 (2017).
[24] Y. Yu, X. Chen, X. Liu, J. Li, B. Sanyal, X. Kong, F. M. Peeters, and L. Li, Phys. Rev. B **105**, 024407 (2022).
[25] R.-W. Zhang, Z. Zhang, C.-C. Liu, and Y. Yao, Phys. Rev. Lett. **124**, 016402 (2020).
[26] G. Ding, J. Wang, H. Chen, X. Zhang, and X. Wang, J. Mater. Chem. C **10**, 6530 (2022).
[27] Y. Jiao, F. Ma, C. Zhang, J. Bell, S. Sanvito, and A. Du, Phys. Rev. Lett. **119**, 016403 (2017).
[28] L. Zhang, S. F. Zhang, W. X. Ji, C. W. Zhang, P. Li, P. J. Wang, S. S. Li, and S. S. Yan, Nanoscale **10**, 20748 (2018).
[29] R. W. Zhang, X. D. Zhou, Z. Y. Zhang, D. S. Ma, Z. M. Yu, W. X. Feng, and Y. G. Yao, Nano Lett. **21**, 8749 (2021).
[30] A series of 2D materials were predicted as SGSs with "Dirac points" at the Fermi level. It is worth noting that linearly dispersed band crossing points in 2D materials are mostly referred to as the "Dirac point" in the literature [20–22]. This is most likely because of its use in early graphene research [31]. Each band crossing point at K or K_0 in graphene is characterized by a 2D Weyl Hamiltonian with a defined chirality, indicating that it is a Weyl point. Although it is conceptually more consistent to call the 2D Dirac point SGSs as 2D Weyl point SGSs, in this Letter, we choose to follow the common practice to use "Dirac point" SGSs in 2D materials.
[31] K. S. Novoselov, A. K. Geim, S. V. Morozov, D. Jiang, M. I. Katsnelson, I. V. Grigorieva, S. V. Dubonos, and A. A. Firsov, Nature (London) **438**, 197 (2005).

[32] In Ref. [25], Zhang *et al.*, proposed two of the simplest types of topological nodal line spin-gapless semimetals (TNLSGSMs). For type-A TNLSGMs, the concentric loops come from different spin channels separately. For type-B TNLSGSMs, the nodal lines come from a single spin channel. Type-B TNLSGSMs can also be viewed as NLSGSs based on the definition of a SGS in 2008 by Wang [9]. In this Letter, we choose to follow the earliest definition to use NLSGSs instead of NLSGSMs.

[33] R. Von der Mühll, D. Dumora, J. Ravez, and P. Hagenmuller, J. Solid State Chem. **2**, 262 (1970).

[34] See Supplemental Material at http://link.aps.org/supplemental/10.1103/PhysRevB.106.L060407 for the calculated methods, magnetic Weyl nodal line and quadratic nodal line states, effects of the on-site Hubbard Coulomb interaction and the uniform strains for the band crossing points, and effects of SOC for the band crossing points, which includes Refs. [25,27,35–61,63].

[35] G. Kresse and J. Furthmüller, Phys. Rev. B **54**, 11169 (1996).

[36] J. P. Perdew, K. Burke, and M. Ernzerhof, Phys. Rev. Lett. **77**, 3865 (1996).

[37] P. E. Blöchl, Phys. Rev. B **50**, 17953 (1994).

[38] Q. Wu, S. Zhang, H.-F. Song, M. Troyer, and A. A. Soluyanov, Comput. Phys. Commun. **224**, 405 (2018).

[39] A. A. Mostofi, J. R. Yates, Y.-S. Lee, I. Souza, D. Vanderbilt, and N. Marzari, Comput. Phys. Commun. **178**, 685 (2008).

[40] Z.-M. Yu, Z. Zhang, G.-B. Liu, W. Wu, X.-P. Li, R.-W. Zhang, S. A. Yang, and Y. Yao, Sci. Bull. **67**, 375 (2022).

[41] X. Zhang, Z.-M. Yu, X.-L. Sheng, H. Y. Yang, and S. A. Yang, Phys. Rev. B **95**, 235116 (2017).

[42] H. Huang, J. Liu, D. Vanderbilt, and W. Duan, Phys. Rev. B **93**, 201114(R) (2016).

[43] X. M. Zhang, L. Jin, X. F. Dai, and G. D. Liu, J. Phys. Chem. Lett. **8**, 4814 (2017).

[44] Y. Kim, B. J. Wieder, C. L. Kane, and A. M. Rappe, Phys. Rev. Lett. **115**, 036806 (2015).

[45] X. Zhang, B. Fu, L. Jin, X. Dai, G. Liu, and Y. Yao, J. Phys. Chem. C **123**, 25871 (2019).

[46] L. M. Schoop, M. N. Ali, C. Straßer, A. Topp, A. Varykhalov, D. Marchenko, V. Duppel, S. S. P. Parkin, B. V. Lotsch, and C. R. Ast, Nat. Commun. **7**, 11696 (2016).

[47] F. Tran and P. Blaha, Phys. Rev. Lett. **102**, 226401 (2009).

[48] M. Zeng, C. Fang, G. Chang, Y.-A. Chen, T. Hsieh, A. Bansil, H. Lin, and L. Fu, arXiv:1504.03492.

[49] B. Feng, B. Fu, S. Kasamatsu, S. Ito, P. Cheng, C.-C. Liu, Y. Feng, S. Wu, S. K. Mahatha, P. Sheverdyaeva *et al.*, Nat. Commun. **8**, 1007 (2017).

[50] C. Xu, Y. Wang, R. Han, H. Tu, and Y. Yan, New J. Phys. **21**, 033005 (2019).

[51] Y. Xu, Y. Gu, T. Zhang, C. Fang, Z. Fang, X.-L. Sheng, and H. Weng, APL Mater. **7**, 101109 (2019).

[52] G. D. Liu, L. Jin, X. F. Dai, G. F. Chen, and X. M. Zhang, Phys. Rev. B **98**, 075157 (2018).

[53] X. M. Zhang, L. Jin, X. F. Dai, G. F. Chen, and G. D. Liu, J. Phys. Chem. Lett. **9**, 5358 (2018).

[54] Y. Du, F. Tang, D. Wang, L. Sheng, E.-J. Kan, C.-G. Duan, S. Y. Savrasov, and X. Wan, npj Quantum Mater. **2**, 3 (2017).

[55] L. Jin, X. M. Zhang, X. F. Dai, L. Y. Wang, H. Y. Liu, and G. D. Liu, IUCrJ **6**, 688 (2019).

[56] J. L. Lu, W. Luo, X. Y. Li, S. Q. Yang, J. X. Cao, X. G. Gong, and H. J. Xiang, Chin. Phys. Lett. **34**, 057302 (2017).

[57] Q. Xu, R. Yu, Z. Fang, X. Dai, and H. Weng, Phys. Rev. B **95**, 045136 (2017).

[58] L. Jin, X. M. Zhang, T. L. He, W. Z. Meng, X. F. Dai, and G. D. Liu, Appl. Surf. Sci. **520**, 146376 (2020).

[59] F. Zhou, Y. Liu, J. Wang, M. Kuang, T. Yang, H. Chen, X. Wang, and Z. Cheng, Phys. Rev. Materials **5**, 074201 (2021).

[60] S. Li, Y. Liu, B. Fu, Z.-M. Yu, S. A. Yang, and Y. Yao, Phys. Rev. B **97**, 245148 (2018).

[61] T. He, X. Zhang, Y. Liu, X. Dai, G. Liu, Z.-M. Yu, and Y. Yao, Phys. Rev. B **102**, 075133 (2020).

[62] X.-L. Wang, S. X. Dou, and C. Zhang, NPG Asia Mater. **2**, 31 (2010).

[63] Z. Zhang, Z. M. Yu, and S. A. Yang, Phys. Rev. B **103**, 115112 (2021).

[64] The spin-polarization ratio can be calculated via the formula as follows, $P = \frac{N\uparrow(E_F)-N\downarrow(E_F)}{N\uparrow(E_F)+N\downarrow(E_F)}$, where $N\uparrow(E_F)$ and $N\downarrow(E_F)$ are the spin-up and spin-down electrons at the Fermi level (E_F), respectively. One finds that $N\uparrow(E_F) = 0$, and thus Sr_2CuF_6 should be fully spin polarized around E_F.

[65] T. L. He, Y. Liu, L. Tian, X. M. Zhang, W. Z. Meng, X. F. Dai, and G. D. Liu, Phys. Rev. B **103**, 085135 (2021).

[66] S.-S. Wang, Y. Liu, Z.-M. Yu, X.-L. Sheng, and S. A. Yang, Nat. Commun. **8**, 1844 (2017).

[67] H. Zhang, X. Zhang, T. He, X. Dai, Y. Liu, G. Liu, L. Wang, and Y. Zhang, Phys. Rev. B **102**, 155116 (2020).

[68] Z. Wang, A. Alexandradinata, R. J. Cava, and B. A. Bernevig, Nature (London) **532**, 189 (2016).

[69] J.-Z. Ma, C.-J. Yi, B. Q. Lv, Z. J. Wang, S.-M. Nie, L. Wang, L.-Y. Kong, Y.-B. Huang, P. Richard, P. Zhang *et al.*, Sci. Adv. **3**, e1602415 (2017).

[70] L. Wu, F. Tang, and X. Wan, Phys. Rev. B **102**, 035106 (2020).

[71] W. Wu, Y. Liu, S. Li, C. Zhong, Z.-M. Yu, X.-L. Sheng, Y. X. Zhao, and S. A. Yang, Phys. Rev. B **97**, 115125 (2018).

[72] S. Z. Chen, S. Li, Y. Chen, and W. Duan, Nano Lett. **20**, 5400 (2020).

[73] Z.-M. Yu, W. Wu, Y. X. Zhao, and S. A. Yang, Phys. Rev. B **100**, 041118(R) (2019).

[74] C. Zhong, Y. Chen, Y. Xie, S. A. Yang, M. L. Cohen, and S. Zhang, Nanoscale **8**, 7232 (2016).

[75] Q.-F. Liang, J. Zhou, R. Yu, Z. Wang, and H. Weng, Phys. Rev. B **93**, 085427 (2016).

[76] Y. Yang, J.-P. Xia, H.-X. Sun, Y. Ge, D. Jia, S.-Q. Yuan, S. A. Yang, Y. Chong, and B. Zhang, Nat. Commun. **10**, 5185 (2019).

[77] M. Xiao, L. Ye, C. Qiu, H. He, Z. Liu, and S. Fan, Sci. Adv. **6**, eaav2360 (2020).

[78] B.-B. Fu, C.-J. Yi, T.-T. Zhang, M. Caputo, J.-Z. Ma, X. Gao, B. Lv, L.-Y. Kong, Y.-B. Huang, P. Richard *et al.*, Sci. Adv. **5**, eaau6459 (2019).

[79] I. I. Mazin, Phys. Rev. Lett. **83**, 1427 (1999).

[80] B. Q. Lv, T. Qian, and H. Ding, Rev. Mod. Phys. **93**, 025002 (2021).

[81] J. Wang, X. Sui, S. Gao, W. Duan, F. Liu, and B. Huang, Phys. Rev. Lett. **123**, 206402 (2019).